JGR Solid Earth

Key Points:
- Stress inversions of slow slip events imply the presence of intrinsically weak fault materials
- The strength of the megathrust is similar to its surroundings in SSE source regions
- Slow fault slip accommodates a large fraction of the total seismic moment in the Nankai Trough

Correspondence to:
T. Newton,
tnewton@uoregon.edu

Stress Orientations in the Nankai Trough Constrained Using Seismic and Aseismic Slip

Tyler J. Newton[1] (ID) and Amanda M. Thomas[1] (ID)

[1]Department of Earth Sciences, University of Oregon, Eugene, OR, USA

Abstract The strength of subduction thrust faults is key to understanding seismogenesis at the provenance of Earth's largest earthquakes. Earthquake focal mechanisms are routinely inverted to constrain the stress state at seismogenic depths. However, on some megathrusts, deformation is accommodated by both earthquakes and types of slow fault slip. We employ focal mechanisms of short-term slow slip events (SSEs), a type of slow fault slip, and earthquakes in a regional stress inversion to investigate the stress state of the Nankai Trough megathrust and interpret the results in the context of regional tectonics Previous studies using earthquake-only stress inversions found principal stress orientations in this region that are incompatible with thrust faulting on the megathrust. When both SSEs and earthquakes are considered, the stress state of the central and eastern Nankai Trough megathrust is well oriented for thrust faulting. Our results suggest that slow fault slip source regions may appear to have misoriented stress fields if slow fault slip constitutes a substantial proportion of fault slip and the stress field is not well constrained by earthquakes. In the SSE region, we find that faults are well oriented for failure, suggesting they have strengths similar to their surroundings. Combined with low Vp/Vs ratios and sensitivity to small stress changes, our results imply that the megathrust and surroundings operate at low deviatoric stresses in the SSE source region. Further, we show that the coefficient of friction for areas hosting SSEs is low ($\mu = 0.19$–0.50), implying frictionally weak materials in the SSE source region.

1. Introduction

Earthquakes are caused by tectonic stresses that govern the type of faulting. The orientation of a tectonic stress field can be described by the three orthogonal principal stresses, σ_1, σ_2, and σ_3, where $\sigma_1 \geq \sigma_2 \geq \sigma_3$ and compression is defined as positive. These principal stresses are, by definition, oriented such that the shear stress on the plane normal to each principal stress is zero. Tectonic stresses accumulate during the interseismic period and are rapidly released as fault slip (Reid, 1910). Anderson (1951) proposed that in an idealized tectonic setting (i.e., absent of topographic stresses), thrust, normal, and strike-slip faults develop in conformance with Mohr-Coulomb yield criterion, with one principal stress axis near vertical because Earth's surface is a boundary with no shear stress. Well-oriented faults composed of rocks with typical friction coefficients ($\mu = 0.6$–0.85 Byerlee, 1978) form and reactivate with the same sense of slip when σ_1, the maximum compressive stress axis, is oriented $\approx 30°$ from the fault plane (Sibson, 1985). Slip on a poorly oriented fault with a high ($> 60°$) or low ($< 10°$) angle of σ_1 to the fault plane (and a typical friction coefficient) is less mechanically favorable than the generation of a new well-oriented fault (Sibson, 1985). The occurrence of slip on poorly oriented faults implies either that the tectonic stress orientation is not well constrained or the fault must be considerably weaker, having a lower apparent coefficient of friction, than its surroundings (Hill, 1993). Thus, the orientation of a stress field relative to faults within it can be used as a proxy for fault strength, assuming the stress field is well constrained.

In areas with abundant fault slip data, earthquake focal mechanisms can be used to constrain the tectonic stress field (Maury et al., 2013). Stress inversions solve for a deviatoric stress tensor that best describes the distribution of slip vectors determined from earthquake focal mechanisms. The inverse problem is commonly solved by grid-search methods (Arnold & Townend, 2007; Gephart, 1990; Gephart & Forsyth, 1984), linearized least-squares methods (Hardebeck & Michael, 2006; Michael, 1984), and Monte Carlo-based methods (Angelier, 1984). Focal mechanism inversion methods assume fault slip occurs in the same direction as the resolved shear stress (i.e., the tangential component of the traction vector) (Bott, 1959; Wallace, 1951), the stress field is homogeneous in each discretized domain, fault slip occurs on preexisting faults, and that the considered focal mechanisms are sufficiently diverse to constrain the
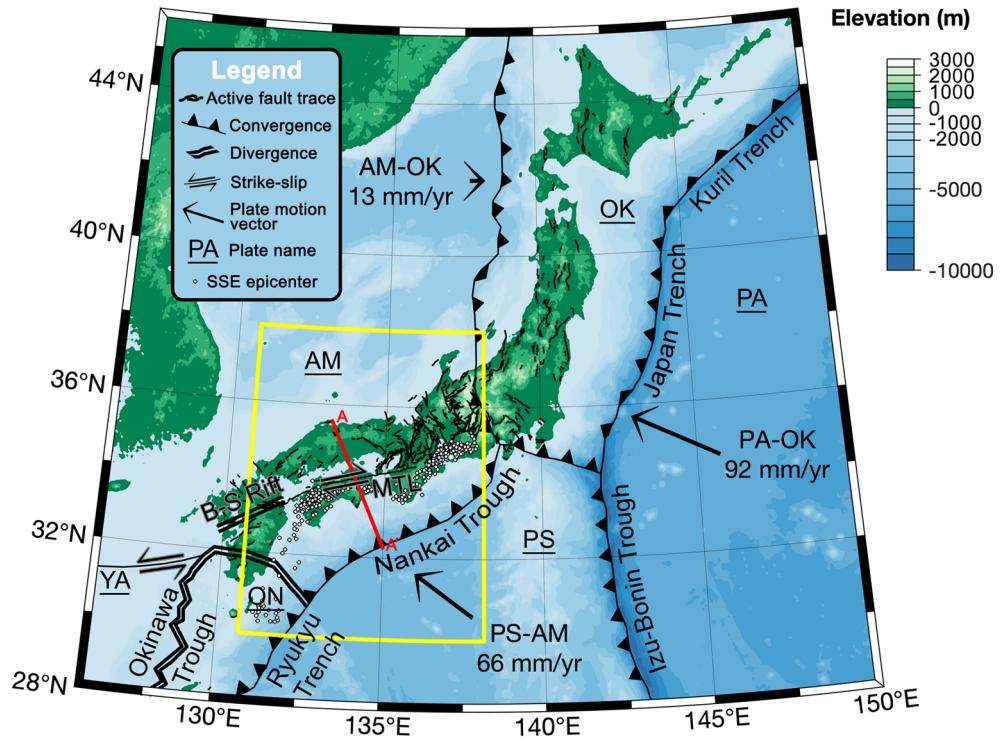
Figure 1. The tectonic setting of Japan. Yellow box denotes the study area. The dominant tectonic features in the Nankai Trough are the Median Tectonic Line (MTL), a right-lateral strike-slip fault, the subducting Philippine Sea plate (PS), the overriding Amur plate (AM), and the Beppu-Shimabara (B-S) rift. The Pacific plate (PA) subducts under the Okhotsk plate (OK) to the north and the Philippine Sea plate to the south. AM-OK subduction forms an incipient subduction zone. To the south, PS subducts beneath the Okinawa plate (ON), adjacent to the Okinawa Trough, a backarc rift. The Okinawa Trough is bordered on the west by the Yangtze plate (YA). Locations of slow slip events considered in this study are denoted by white circles with black outlines. Active fault traces from AIST Research Information Database DB095: Active fault database of Japan (2012). Plate boundaries from Kita et al. (2001) and Bird (2003).

stress field (McKenzie, 1969). The magnitude of fault slip is not considered in the inversion, so principal stress directions rather than absolute stress values are calculated from the deviatoric stress tensor. However, quantitative models have been developed to estimate in situ stresses from earthquake focal mechanisms in conjunction with high-density borehole stress measurements (Shen et al., 2019). Earthquake focal mechanisms intrinsically contain fault plane ambiguity, so inversions that do not distinguish the fault plane from the auxiliary plane may produce inaccurate results. Vavryčuk (2014) modified the Michael (1984) method to invert jointly for stress and fault orientation, where the nodal plane closest to failure, based on the fault instability coefficient (Lund & Slunga, 1999; Vavryčuk et al., 2013), is selected as the fault plane. If the focal mechanisms utilized in a stress inversion do not accurately sample the tectonic stress field, the calculated deviatoric stress tensor will be misoriented. Martínez-Garzón et al. (2016) detailed a best practice methodology for stress inversions of earthquake focal mechanisms and suggested that aftershock sequences be removed from focal mechanism catalogs so the assumption of stress field homogeneity is not violated by considering internal stress perturbations of earthquake clusters. In this study, we employ stress inversion best practices to determine the spatially variable stress field of the subduction interface in the Nankai Trough region of Japan.

The tectonic setting of Japan is unique in that southwestern Japan hosts subduction of the Philippine Sea plate (PS) beneath the Amur plate (AM) at 63–68 mm year^{-1} N55°W near the Nankai Trough (Miyazaki & Heki, 2001) while in northeastern Japan the Pacific plate (PA) subducts beneath the Okhotsk plate (OK) (Zonenshain & Savostin, 1981) at 92 mm year^{-1} N66°W (DeMets et al., 2010), creating the Kuril arc and the Japan arc (Figure 1). Convergence of PS-AM is oblique, causing migration of the Nankai forearc sliver to the west. The Nankai forearc sliver is bounded on the north by the Median Tectonic Line (MTL), a

right-lateral strike-slip fault with an average slip-rate of 5–8 mm year^{-1} (Tsutsumi et al., 1991). The Ryukyu arc, associated with subduction of the PS beneath the ON, hosts an actively rifting backarc basin, the Okinawa Trough, which decouples the forearc and generates arc-parallel extension (Kubo & Fukuyama, 2003). The Beppu-Shimabara rift transects the island of Kyushu and has been interpreted by Tada (1985) to be a northern extension of the Okinawa Trough. The majority of the seismicity in Japan is associated with PA-OK subduction in the northeast (Figure S1 in the supporting information). The Nankai Trough hosts predominantly small (M < 5) thrust earthquakes due to active subduction of the PS beneath the AM and right lateral strike-slip earthquakes due to the proximity of the MTL (Figure S1). The Nankai Trough generated a M_w8.1 earthquake in 1944 and a M_w8.3 earthquake in 1946 (Usami, 1996).

Previous studies that have estimated stress orientations in the Nankai Trough are based on borehole observations and the inversion of earthquake focal mechanisms or fault orientations. The Kii Peninsula has been the site of numerous studies that find σ_1 oriented nearly vertical to 2 km depth (Byrne et al., 2009; Lin et al., 2016; Sacks et al., 2013), suggesting that topographic gradients are a dominant control on the shallow crustal stress state. Townend and Zoback (2006) and Terakawa and Matsu'ura (2010) conducted stress inversions of focal mechanisms shallower than 35 and 50 km, respectively, finding that the orientation of the maximum horizontal compressive stress is dominantly oriented E-W across Japan (due to AM-OK convergence) but varies throughout the Nankai Trough due to the complicated tectonics of the region (and potentially the low seismicity rate). Wang et al. (2004) and Lee et al. (2017) examined focal mechanism solutions in the Nankai Trough, similarly finding E-W compression throughout the Nankai Trough, and downdip tension near Kyushu. Conversely, Ito et al. (2009) derived moment tensor solutions for shallow very-low-frequency (VLF) earthquakes and inverted them to find that σ_1 is trench-normal in the Nankai Trough accretionary prism, indicating that types of fault slip other than traditional earthquakes are useful to constrain the stress field in low-seismicity areas.

Multiple prior studies using focal mechanism stress inversions of the megathrust have revealed principal stress orientations in the Nankai Trough subduction zone that are misoriented for thrust faulting (Hardebeck, 2015; Hardebeck & Loveless, 2018). Hardebeck (2015) investigated principal stress orientations in subduction zones globally to find that in most subduction zones the maximum compressive stress axis plunges trenchward and makes an angle of 45°–60° to the subduction megathrust. However, in the Nankai Trough, Hardebeck (2015) and Hardebeck and Loveless (2018) found maximum compressive stress axis orientations at negative and high angles to the subduction megathrust, differing by >80° in adjacent bins, that are misoriented for thrust faulting. Hardebeck and Loveless (2018) inverted earthquake focal mechanisms across Japan to determine the deviatoric megathrust stress field and found that creeping areas of the Nankai Trough and Japan Trench subduction zones host principal stress orientations that are more poorly oriented for failure than adjacent locked areas. The stress field in an active tectonic margin determines the preferred faulting mechanism in that area, so regions with principal stress orientations incompatible with the observed type of faulting require a physical explanation of such a discrepancy. Hardebeck (2015) attributed the seemingly misoriented principal stress orientations of the Nankai Trough subduction zone to high pore fluid pressure and regionally low deviatoric stress.

An observation of relevance to this study is that the regions with stress fields that are poorly oriented for megathrust faulting found in previous studies are spatially coincident with areas of observed and inferred slow fault slip (Figure S7 Hardebeck & Loveless, 2018). Over the past two decades, analyses of geodetic and seismic time series have revealed various types of slow fault slip in the Nankai Trough subduction zone (Hirose & Obara, 2005; Katsumata & Kamaya, 2003; Obara, 2002; Obara et al., 2004), and other faults globally (Brown et al., 2009; Dragert et al., 2001; Nadeau & Dolenc, 2005; Payero et al., 2008; Rogers & Dragert, 2003), that slip over a range of spatial and temporal scales. Slow slip events (SSEs) constitute distinguishable geodetic episodes of slow fault slip with durations of days to years. VLF earthquakes are slow earthquakes with characteristic time scales of tens of seconds. Low-frequency earthquakes and tremor are another manifestation of slow fault slip that occurs in the Nankai Trough with a dominant frequency of several Hz (Obara, 2002; Shelly et al., 2007). Episodes of tremor have been found to accompany VLF earthquakes and short-term SSEs (Obara et al., 2004; Rogers & Dragert, 2003), which is termed episodic tremor and slip (ETS). The occurrence of slow fault slip, or creep, in subduction zones varies spatially and temporally along strike and dip and can occur both updip and downdip of the seismogenic zone where earthquakes nucleate.
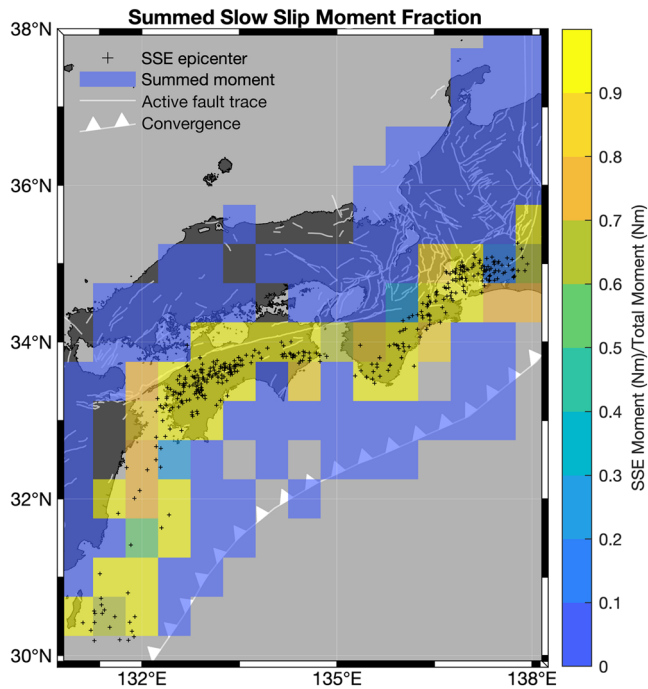
Figure 2. The fraction of summed moment from 1997 to 2015 for arbitrary 0.5° bins of SSEs considered in this study to the total summed moment of earthquakes and SSEs. In each bin that SSEs are pervasive, SSEs constitute the majority of the summed moment. We use a shear modulus of 30 GPa and inversion-derived fault parameters to calculate the moment of slow slip events. Earthquake moments are sourced from the NIED F-Net catalog. Active fault traces from AIST Research Information Database DB095: Active fault database of Japan (2012).

Tremor and ETS occur in a narrow zone along the downdip edge of the megathrust seismogenic zone in Nankai, while long-term SSEs fill the gap between ETS and the seismogenic zone (Kobayashi, 2014). Shallow VLF earthquakes and short-term SSEs occur updip of the seismogenic zone in this region (Obara & Ito, 2005). Yokota et al. (2016) revealed that areas of slow fault slip bound areas of historic megathrust slip. Various studies have inferred high pore fluid pressures in areas of the Nankai Trough that spatially coincide with shallow slow fault slip (Takemura et al., 2019; Tobin & Saffer, 2009; Ujiie et al., 2018). Friction experiments on materials from the shallow megathrust in the Nankai Trough (Brown et al., 2003; Ikari et al., 2009; Kopf & Brown, 2003), and from faults globally (Bürgmann, 2018; Collettini et al., 2019), reveal low-strength materials; however, the sampling of in situ megathrust materials at the depths of downdip SSEs is not feasible with current methods. In the Hikurangi margin, Warren-Smith et al. (2019) observed temporal evolution of the stress shape ratio in subducting oceanic crust that temporally correlates with SSEs, interpreted as fluid pressure cycling, providing further evidence that the presence of fluids at high pore pressures is a control on the nucleation of SSEs.

Interestingly, the Nankai trough hosts less earthquakes and more slow fault slip than adjacent areas (Figure S1), so SSEs make up a substantial portion of the moment budget in this area (Figure 2). Figure 2 shows the fraction of summed SSE moment to total summed moment including both earthquakes and SSEs, where all events that occur within arbitrary 0.5° bins contribute to the moment sum of that bin. SSEs constitute the majority of the total moment in the Nankai Trough, even if a very conservative shear modulus (1 GPa) is used to constrain the lower bound of SSE moment fraction. Stress orientations based on focal mechanism inversions estimate the deviatoric stress tensor of the sampled volume; therefore, regional principal stress analyses of the subduction zone interface should include all substantial sources of megathrust slip for which focal mechanisms can be resolved, as different types of fault slip occupy different volumes of the fault interface. SSEs are generally not represented in focal mechanism catalogs and are therefore excluded from stress inversions. To date, no studies have introduced focal mechanisms of slow fault slip in conjunction with earthquakes into spatially variable regional stress analyses to further constrain the tectonic stress field. In this paper, we investigate the stress orientations in the Nankai Trough while considering both earthquakes and slow fault slip along the subduction interface. We invert SSE focal mechanisms in conjunction with a standard moment tensor catalog to estimate the best-fitting spatially variable stress field and its relationship to the megathrust geometry.

2. Data and Methods

2.1. Focal Mechanism Catalog Processing

We perform stress inversions of 368 short-term SSE focal mechanisms compiled from Sekine et al. (2010), Nishimura et al. (2013), Nishimura (2014), and Kano et al. (2018). Sekine et al. (2010) estimated fault parameters for short-term SSEs occurring from 2001 to 2008 by inverting tiltmeter data for events recorded by at least four stations near the source, resulting in the detection of 54 SSEs with moment magnitudes of 5.4 to 6.2. The SSEs detected by Sekine et al. (2010) have a recurrence interval of approximately 6 months, and each event accommodated approximately 1 cm of slip. Nishimura et al. (2013) detected short-term SSEs from June 1996 to January 2012 along the Nankai Trough, ranging in moment magnitude from 5.5 to 6.3, by identifying displacement reversals in the convergence-parallel component of GNSS (Global Navigation Satellite System) data in addition to estimating fault parameters for the detected SSEs using the nonlinear inversion method of Matsu'ura and Hasegawa (1987). Similarly, Nishimura (2014) applied the method of Nishimura et al. (2013) to data from 352 continuous GNSS stations spanning January 1997 to November 2013 to detect SSEs ranging in moment magnitude from 5.6 to 6.8 and estimate their fault parameters. The data made available by Kano

et al. (2018) in the Science of Slow Earthquakes Slow Earthquake Database include the work of Kitagawa et al. (2011, 2012), Itaba et al. (2012, 2013a, 2013b), Itaba, Koizumi, Takahashi, Matsumoto, Kitagawa, Takeda, et al. (2014), Itaba, Koizumi, Takahashi, Matsumoto, Kitagawa, Ochi, et al. (2014), and Ochi et al. (2015, 2016) from reports of the Coordinating Committee for Earthquake Prediction in Japan, which includes detected SSEs and their fault parameters spanning February 2011 to December 2015. SSE focal mechanisms from Sekine et al. (2013a), Kitagawa et al. (2011, 2012), Itaba et al. (2012, 2013a, 2013b, 2013b), Itaba, Koizumi, Takahashi, Matsumoto, Kitagawa, Takeda, et al. (2014), Itaba, Koizumi, Takahashi, Matsumoto, Kitagawa, Ochi, et al. (2014), and Ochi et al. (2015) are derived from models that fix the fault plane to the plate boundary and define the slip direction as the direction of plate convergence. In contrast, Nishimura et al. (2013) and Nishimura (2014) fix the fault plane to the plate boundary but include slip as a free parameter. Duplicate SSEs detected by more than one study are removed from the compiled SSE catalog. We consider only events within the study area shown in Figure 1. The magnitude of completeness of the NIED catalog is approximately 3.8 (Kubo et al., 2002). In contrast, all SSEs with a magnitude <6 are not expected to be completely recovered by geodetic studies (Nishimura et al., 2013). Given that slow fault slip is expected to follow a Gutenburg-Richter frequency-magnitude distribution (Gutenberg & Richter, 1944; Wech et al., 2010), Figure 2 represents a minimum estimate of the summed SSE moment and a minimum bound on the contribution of SSEs to total moment.

Additionally, we perform stress inversions of 1,229 earthquake focal mechanisms from the National Research Institute for Earth Science and Disaster Resilience (NIED) F-net moment tensor catalog (Okada et al., 2004). The NIED catalog is truncated to have the same temporal span as the compiled SSE catalog, from 22 January 1997 to 30 December 2015. Martínez-Garzón et al. (2016) demonstrated that clustered seismicity in earthquake catalogs biases the results of stress inversions. Therefore, we decluster the NIED earthquake catalog and compiled SSE catalog using SEDA (Lombardi, 2017), a tool for Epidemic Type Aftershock Sequence (ETAS) declustering (Zhuang et al., 2002). The ETAS declustering method of Zhuang et al. (2002) uses a space-time branching process model to distinguish persistent background earthquake activity from aftershock sequences and earthquake swarms that are clustered in time and space, by means of a maximum likelihood estimation. Declustering the catalogs minimizes the inclusion of events triggered by local stress perturbations in our analysis of the stress field surrounding the megathrust. The earthquake catalog is then filtered to contain only events within 10 km of the megathrust, as determined by Hayes et al. (2018), and above 60 km depth. We use a 10 km envelope around the megathrust to avoid including seismicity originating from the MTL and other crustal faults in our analysis of the megathrust stress field (Figure S2).

Binning the data is necessary to investigate spatial variation in the stress field. Previous studies (Hardebeck & Michael, 2004) have shown that varying interpretations of results from the same focal mechanism data set result from different binning schemes (e.g., Hardebeck & Hauksson, 1999; Townend & Zoback, 2001). Here, we determine bins using k-means++ clustering (Arthur & Vassilvitskii, 2006) of epicenters and require a minimum cluster size of 50 events to minimize the uncertainty associated with the inversion and provide robust estimates of the stress field orientation for the spatial extent of each cluster. We perform three different inversions to explore the effect of SSEs on the calculated stress field, one containing only earthquake focal mechanisms from the NIED catalog, one containing only SSE focal mechanisms, and one containing both SSE focal mechanisms and earthquake focal mechanisms. The number of clusters for each inversion was selected to generate clusters containing between 50 and 70 events. The filtered earthquake catalog is discretized into 21 clusters with a mean cluster size of 57 events. The compiled SSE catalog is discretized into six clusters with a mean cluster size of 61 events. The catalog containing earthquakes and short-term SSEs is discretized into 30 clusters with a mean cluster size of 53 events. Since each inversion contains clusters of unique dimensions, we facilitate comparison between the earthquake-only and the earthquake-and-SSE inversion results by designating groups of clusters that span similar spatial areas, labeled EI#, for groups from the earthquake-only inversion, and ESI# for groups from the earthquake and SSE inversion. We utilize Kaverina-type rupture classification diagrams (Kagan, 2005; Kaverina et al., 1996) generated by FMC (Álvarez-Gómez, 2019) to visualize the rupture type of focal mechanism data to determine each group. Kaverina-type ternary diagrams classify events into seven rupture types based on the plunges of the P, B, and T centroid moment tensor axes: (1) strike-slip; (2) strike-slip–normal; (3) strike-slip–reverse; (4) normal–strike-slip; (5) reverse–strike-slip; (6) normal; and (7) reverse (Figure 3). Groups were determined
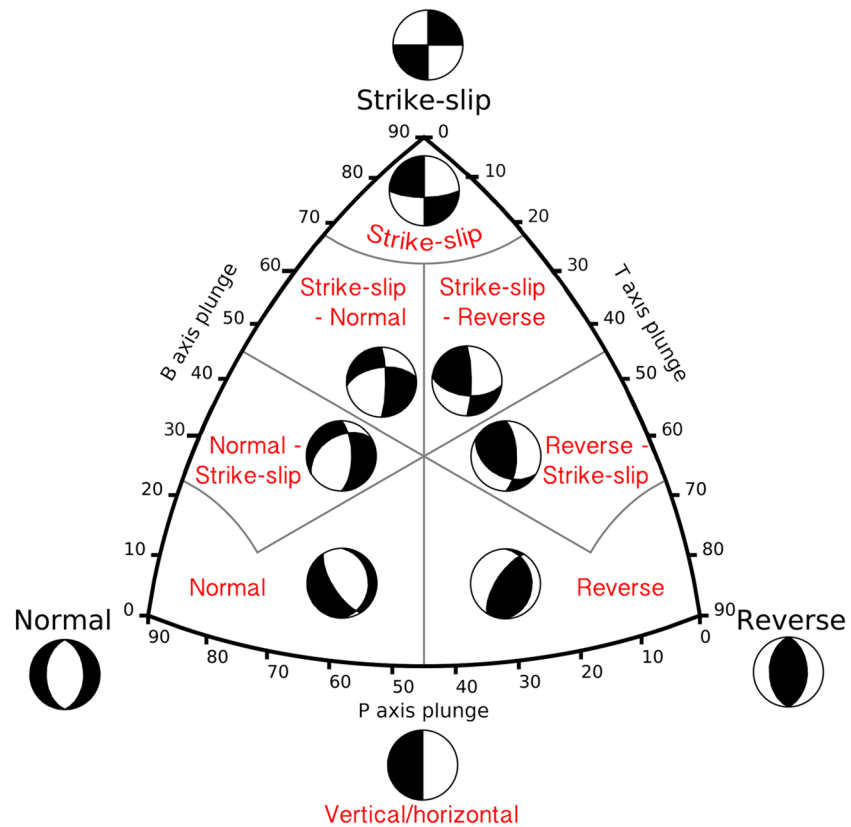
Figure 3. The Kaverina rupture type classification ternary diagram used in this study to visualize the sense of slip, which classifies events into seven types as a function of the plunges of the P, B, and T centroid moment tensor axes computed from the deviatoric moment tensor (modified from Álvarez-Gómez, 2019).

by including adjacent clusters that have similar Kaverina classification diagrams (i.e., they include similar focal mechanism distributions).

2.2. MSATSI

We use MSATSI (Martínez-Garzón et al., 2014), a revised version of the SATSI algorithm (Hardebeck & Michael, 2006), to invert focal mechanisms for the best fitting deviatoric stress tensor of each cluster. SATSI is a damped least-squares inversion algorithm based on the Michael (1984) inversion method. In addition to the assumption shared among all stress inversions that fault slip occurs in the same direction as the shear stress vector (Bott, 1959; Wallace, 1951), Michael (1984) assumes the magnitude of shear stress for all fault slip is similar, which simplifies the inverse problem to a system of linear equations. SATSI expands on the method of Michael (1984) by damping the inversion over spatial and/or temporal dimensions to generate solutions with the minimum complexity necessary to fit the data (Hardebeck & Michael, 2006). A damped inversion allows the model to include heterogeneous solutions for areas where heterogeneity is required by the data and smoothed solutions for areas in which the data do not require heterogeneity by simultaneously inverting for stress orientations in all clusters while minimizing the solution difference between adjacent clusters to better approach a continuous transition between stress states. MSATSI includes minor corrections to the SATSI algorithm and wrapped versions of SATSI for the MATLAB environment (MATLAB, 2018). We select fault planes from auxiliary planes using the method of Vavryčuk (2014), in which the nodal plane with the highest fault instability coefficient is selected as the fault plane; then we perform a 2-D inversion of each data set using MSATSI. Uncertainty is determined by 2,000 iterations of bootstrap resampling of the input data for each cluster, then identifying the bootstrapped data within the 95% confidence intervals.
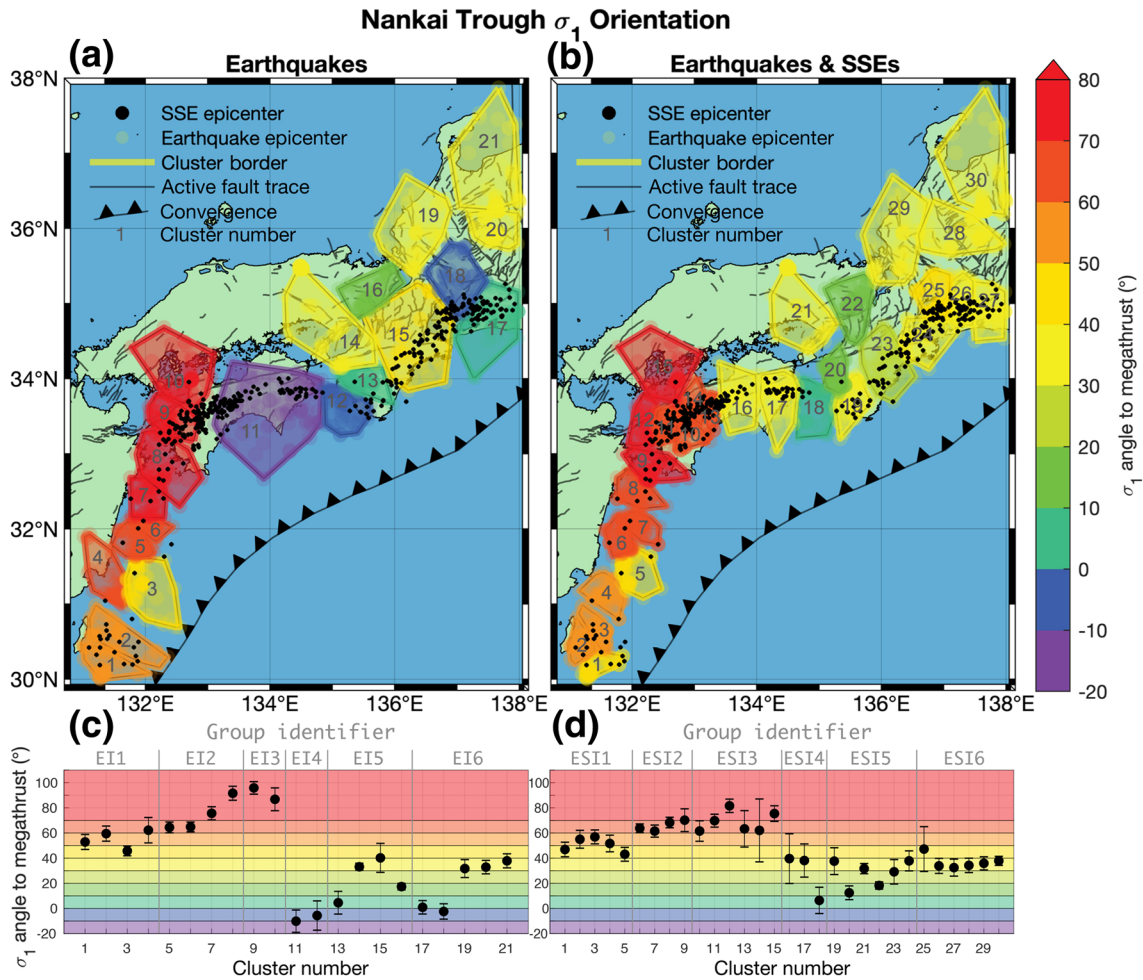
Figure 4. Results of stress inversions for two cases of inputs. (a) Spatial distribution of the orientation of σ_1 to the megathrust for the case of earthquakes only. Cluster numbers are indicated by gray integers. Angles of σ_1 to the megathrust above 80° saturate the colorbar for Clusters 8 and 9. (b) Same as panel (a) but for earthquakes and SSEs. (c) σ_1 to the megathrust versus cluster number for earthquake clusters. Error bars indicate the 95% confidence interval. Groups of clusters that span similar spatial areas between the two inversions are denoted by vertical gray lines and the corresponding group identifier. (d) Same as panel (c) but for earthquakes and SSEs.

3. Results

As described in section 2, we perform three main inversions: one that includes only focal mechanisms from earthquakes, one that includes a regional catalog of SSEs in conjunction with earthquakes, and one that includes only focal mechanisms from SSEs. The results of these analyses are shown in Figures 4 and 6 and are not sensitive to different cluster arrangements, shown in Figure S3. We describe our results in terms of the angle between the mean-local megathrust dip for each cluster and the apparent plunge of σ_1 in the dip direction, as in Figure S2. The plunge of σ_1 is defined as positive if the plunge direction (i.e., the trend) is greater than $\pm 90°$ from the average megathrust dip direction defined by Slab2 (Hayes et al., 2018) for each cluster. The angle of σ_1 to the megathrust and its uncertainty for each cluster are shown in Figures 4c and 4d. Since uncertainties are estimated from bootstrap resampling, higher uncertainties result from groups of slip vectors that are less likely to originate from the same stress field. In general, higher uncertainties in our analysis represent clusters contaminated with focal mechanisms that represent local faulting that differs from regional megathrust activity. We separate clusters from both the earthquake-only and the earthquake and SSE inversions into groups that span similar areas, labeled EI# (Figure 4c) for groups from the earthquake-only inversion and ESI# (Figure 4d) for groups from the earthquake and SSE inversion. Kaverina-type rupture classification diagrams for all events in each group are shown in Figures 5a and 5b.
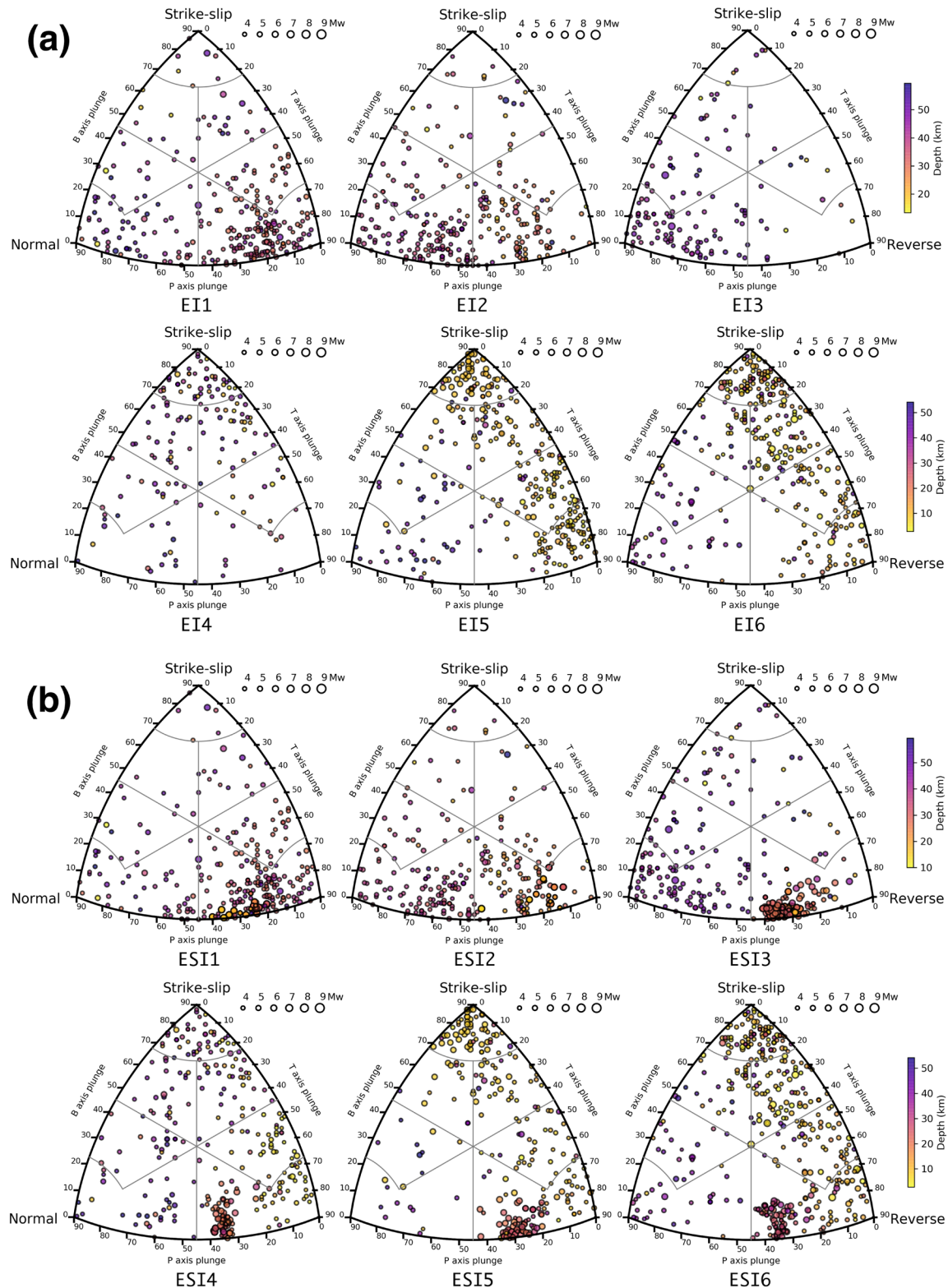
Figure 5. Ternary diagrams of the focal mechanisms comprising (a) Groups EI1 to EI6, identified in Figure 4c, from the earthquake-only inversion, and (b) Groups ESI1 to ESI6, identified in Figure 4d, from the earthquake-and-SSE inversion. Groups that share the same number represent similar spatial areas between the two inversion. SSEs appear as clusters of points. Ternary diagrams generated with FMC (Álvarez-Gómez, 2019). Focal mechanisms are denoted by black-outlined circles filled to indicate event depth in km and sized to indicate the moment magnitude of the event. Refer to Figure 3 for the seven classification types represented in a Kaverina diagram.
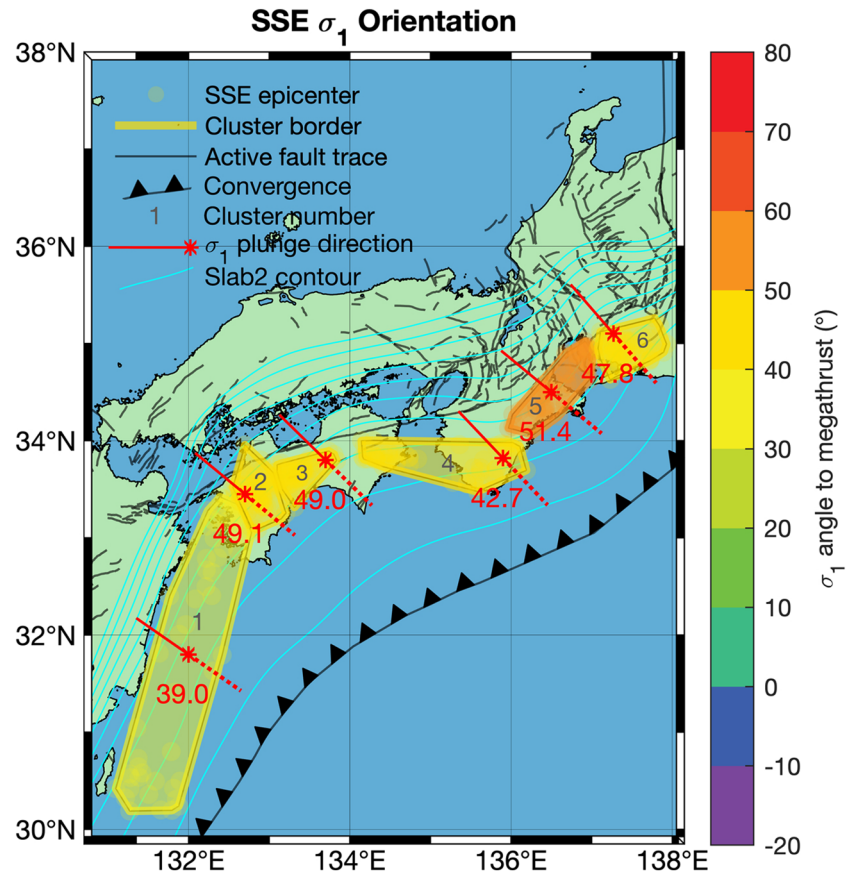
Figure 6. The spatial distribution of the orientation of σ_1 to the megathrust for the case of SSEs only. Clusters numbers are indicated by gray integers. The orientation of σ_1 is denoted by red lines. Red numbers denote the plunge of σ_1 relative to the megathrust, which is also indicated by the colorbar. We use the convention of σ_1 being the most compressive principal stress. 10 to 100 km megathrust depth contours from Hayes et al. (2018) are shown as cyan lines.

When only earthquakes are considered, σ_1 is at intermediate angles to the megathrust ($>40°$ and $\leq60°$) in the western Nankai Trough for Clusters 1–3 (Figure 4a) and at high angles to the megathrust ($>60°$) for Clusters 4–10. Clusters 1–4, denoted as Group EI1 (Figure 4c), predominantly reflect oblique thrust faulting along the megathrust (Figure 5a), transitioning into a zone dominated by extension to the north. Cluster 4 has greater uncertainty than the surrounding clusters, at $\pm10.1°$ for the 95% confidence interval (Figure 4c). Groups EI2 and EI3, composed of Clusters 5–8 and 9–10, respectively, reflect pervasive normal faulting in this area due to the proximity of the Beppu-Shimabara rift (Figure 5a). In Clusters 11, 12, and 18, σ_1 plunges at negative angles to the megathrust. Clusters 11 and 12, grouped as EI4, primarily contain right-lateral strike-slip events, consistent with the sense of slip on the MTL and the sparseness of megathrust seismicity in this area. Cluster 18 includes many left-lateral focal mechanisms, indicative of active local faulting along a network of faults known to host large ($M_w \geq 7.5$) crustal earthquakes (Kaneda & Okada, 2008), rather than activity along the megathrust. Clusters 13 and 17 exhibit low angles of σ_1 to the megathrust ($>0°$ and $\leq10°$). σ_1 plunges at angles $>10°$ and $\leq50°$ to the megathrust in Clusters 14 through 16 and 19 through 21.

When short-term SSEs are considered in conjunction with earthquakes, a larger number of events results in increased spatial resolution of the stress field (Figure 4b). The cluster numbers associated with the inversion shown in Figure 4a identify different spatial areas from those shown in Figure 4b; however, the six cluster groups identified for each inversion in Figures 4c, 4d, 5a, and 5b represent similar spatial areas between inversions. σ_1 is at intermediate angles to the megathrust ($>40°$ and $\leq60°$) for Clusters 1 through 5, denoted as Group ESI1 (Figure 5a), which reflects oblique thrust faulting consistent with the direction of PS-AM

Table 1
SSE Friction Estimates

SSE Cluster[a]	μ
1	0.24
2	0.21
3	0.50
4	0.20
5	0.19
6	0.28

[a]As shown in Figure 6.

convergence. Clusters 6 through 15, which spatially coincide with Clusters 5 through 10 in the earthquake-only inversion, exhibit high angles of σ_1 to the megathrust ($>60°$), though σ_1 to the megathrust may be oriented at ($<60°$) in Clusters 10, 13, and 14 within the bounds of uncertainty (Figure 4d). Similar to Groups EI2 and EI3, Groups ESI2 and ESI3 reflect pervasive normal faulting due to the proximity of the Beppu-Shimabara rift. However, the inclusion of SSEs resolves a thrust component in Group ESI3, which was not resolved in Group EI3. With the exception of Cluster 18, σ_1 plunges at angles $>10°$ and $\leq 50°$ to the megathrust in Clusters 16 through 30; however, Cluster 25 contains significant uncertainty of $\pm 17.8°$. Clu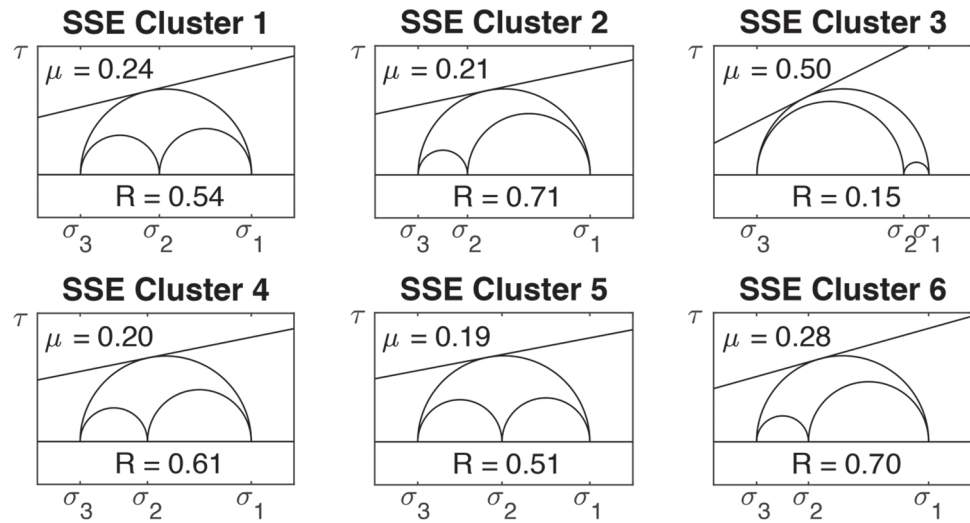ster 25 occupies a similar spatial domain as Cluster 18 in the earthquake-only inversion, an area with active left lateral faulting. Cluster 18 exhibits negative to intermediate angles of σ_1 to the megathrust at the 95% confidence interval. With the inclusion of SSEs, Group ESI4 includes a greater proportion of thrust events rather than being composed of predominately right lateral events as in Group EI4. Both Groups ESI5 and ESI6 experience an increase in the proportion of thrust focal mechanisms over Groups EI5 and EI6.

When only SSEs are considered, σ_1 is well oriented at angles between 39.0° and 51.4° to the megathrust for all clusters (Figure 6). The plunge direction of σ_1 agrees with the megathrust dip direction (i.e., the plunge direction of σ_1 is oriented 180° from the megathrust dip direction) to within $\pm 12.7°$ for all clusters except Cluster 4. In Cluster 4, σ_1 is oriented 36.6° from the mean-local megathrust dip. All SSEs considered have thrust focal mechanisms. The iterative inversion method of Vavryčuk (2014) evaluates the fault instability coefficient of each cluster based on the stress field shape ratio, the orientation of the fault plane to the principal stress axes, and a range of values for overall fault friction, μ. We allow the value for fault friction to span values from 0.01 to 1.00 by a step of 0.01 to determine the value of μ that requires the highest fault instability based on the input focal mechanisms for each cluster. Table 1 shows estimated values of fault friction for all SSE clusters. The estimated apparent fault friction is lowest for Cluster 5, at $\mu = 0.19$, and highest for Cluster 3, at $\mu = 0.50$. To consider the effect of different SSE data sets on the stress inversion results, we perform two additional SSE-only stress inversions for the compiled data set that includes slip direction as a free parameter (Nishimura et al., 2013; Nishimura, 2014) and the compiled data set that fixes the SSE slip direction to the plate convergence direction (Itaba et al., 2012, 2013a, 2013b; Itaba, Koizumi, Takahashi, Matsumoto, Kitagawa, Takeda, et al., 2014; Itaba, Koizumi, Takahashi, Matsumoto, Kitagawa, Ochi, et al., 2014; Kitagawa et al., 2011, 2012; Sekine et al., 2010; and Ochi et al., 2015, 2016). However, Nishimura et al. (2013) and Nishimura (2014) use reversals in plate convergence direction to trigger SSE detection; therefore, both SSE data sets do not include SSEs that are not dominantly reversals of plate convergence. The results presented here are not sensitive to the SSE data set, and Figures S4 and S5 show that similar principal stress orientations are observed for each SSE data set.

4. Discussion

For the earthquake-only inversion, our stress field estimates are similar to those found by Hardebeck (2015) and Hardebeck and Loveless (2018) and include multiple regions where σ_1 is poorly oriented for megathrust faulting (Figure 4a). When focal mechanisms of SSEs, which account for a large fraction of the total moment release in the Nankai Trough, are considered in addition to typical earthquakes, σ_1 more closely approaches the range of angles appropriate for thrust faulting. The area of the largest change in the orientation of σ_1 between the two inversions is Groups EI4/ESI4 (Figure 4a and 4b), where the inclusion of slow fault slip results in the angle between σ_1 and the megathrust changing from negative to positive values consistent with thrust faulting. Due to large ($>30°$) changes in the orientation of σ_1 between the two inversions for Groups EI4 and ESI4, we interpret the negative angles of σ_1 to the megathrust found in our earthquake-only inversion and previous studies (Hardebeck, 2015; Hardebeck & Loveless, 2018) to be products of the low seismicity rate (i.e., few earthquakes are available to constrain the stress state in these areas) and the inclusion of focal mechanisms more closely associated with the MTL (Figures 5a and 5b). In areas where SSEs constitute the majority of the summed moment on a fault, such as the Nankai Trough (Figure 2), the stress field may be poorly constrained if slow fault slip is not considered.

Figure 7. Mohr-Coulomb failure conditions for the SSE clusters shown in Figure 6 determined by iterative stress inversions with a fault instability constraint. R is the shape ratio (Gephart & Forsyth, 1984), where $R = (\sigma_1 - \sigma_2)/(\sigma_1 - \sigma_3)$.

The inclusion of short-term SSEs with earthquakes in the inversion produces high angles of σ_1 to the megathrust in the western Nankai Trough, with improved spatial resolution over the earthquake-only inversion. σ_1 orientations for the western Nankai Trough do not differ significantly between the two data sets (Figures 4a and 4b) and are similar to the results of Hardebeck (2015) and Hardebeck and Loveless (2018). High angles of σ_1 to the megathrust in this region are consistent with prevalent normal faulting from backarc extension (Figures 5a and 5b). The overriding AM of the western Nankai Trough experiences extension from the nearby Okinawa Trough and Beppu-Shimabara rift (Figure 1), in addition to compression from the obliquely subducting PS. Ikeda et al. (2009) proposed stress field segmentation of the MTL on the basis of geological, geophysical, and seismic data, finding the MTL in a state of transpression in the eastern Nankai Trough transitioning to a state of transtension in the western Nankai Trough. Our results support the interpretation of Ikeda et al. (2009) and show that the same stress field segmentation governs faulting in the volume of crust surrounding the megathrust. Our results are consistent with GPS measurements of crustal deformation, which show northwest motion in eastern Nankai Trough transitioning to predominantly southeast motion in the western Nankai Trough (Sagiya et al., 2000). While the inclusion of SSEs does not significantly change the σ_1 orientation in the western Nankai Trough, it does provide insight into the influence of extensional tectonic features on the stress field. The high angles of σ_1 to the megathrust in the western Nankai Trough are a result of the proximity of extensional tectonic features to the subduction margin. This result is further supported by the SSE-only inversion, which results in σ_1 orientations that are optimally oriented for thrust faulting, though the SSE data sets used in this study utilize detection criteria that preclude the detection of SSEs that are not dominantly reversals of the plate convergence direction.

Stress inversions employ catalogs of earthquake focal mechanisms to determine tectonic stress orientations, and since most focal mechanism catalogs exclude SSEs, aseismic slip is not typically included in stress inversions. In regions like the Nankai Trough, SSEs occur both downdip and updip of the seismogenic zone, so their inclusion in stress inversions increases the spatial extent of the data and can be used to determine the stress field in areas where typical earthquakes are sparse or absent. For example, future studies utilizing seafloor observation systems to detect shallow seismicity and slow fault slip may be capable of resolving the megathrust stress field to the trench. Further, future studies may explore methods of constraining the fault slip vector of SSEs beyond convergence-parallel displacement reversals to better constrain the megathrust stress state. Additionally, the resolution of stress inversions is often data limited, and the number of events per bin is selected to achieve a balance between the desired spatiotemporal resolution and model uncertainty. The inclusion of slow fault slip in stress inversions increases the quantity of data, which may

improve the model uncertainty and resolution. To conclude this study, we explore the implications of results from the SSE-only inversion.

4.1. Implications for SSEs

Our results show that the maximum compressive principal stress orientations of all SSE clusters (Figure 6) are 39.0°–51.4° from the megathrust, well oriented for megathrust faulting. Optimally oriented faults with typical friction coefficients make angles between ~25° and ~45° to σ_1 and are thought to have strengths similar to their surroundings. However, some faults are observed to operate at angles to σ_1 that are outside this range. Such faults are called non-optimally oriented and are thought to be much weaker than their surroundings because they slip at low applied shear stress. Our results imply that the strength of the megathrust in regions hosting slow slip is similar to the surrounding material. SSEs often occur in regions of elevated Vp/Vs ratios which are attributed to elevated pore fluid pressures in the SSE source and surrounding regions (Audet & Bürgmann, 2014). Additionally, the extreme sensitivity of slow fault slip to small magnitude dynamic stress changes imparted from earthquakes and tides implies that the megathrust itself is weak in regions hosting slow slip (e.g., Hawthorne & Rubin, 2010; Thomas et al., 2012). These observations are consistent with our results and imply that the megathrust and its surroundings operate at low deviatoric stresses due to the presence of pressurized fluids.

Our fault stability analyses reveal overall fault friction coefficients that are lower than those predicted by Byerlee's law (Table 1). Estimated friction coefficients are determined from the deviatoric stress tensor and are independent of the pore fluid pressure in the SSE source region assuming the same pore fluid pressure modulates each principle stress (Sibson, 1985). As such, the low coefficients of friction for all SSE clusters suggest that frictionally weak materials are present in the SSE source region in the Nankai Trough (e.g., French & Condit, 2019).

To further explore the implications of our results, we consider the principal stress shape ratio and the principal stress orientations (Figure 7), recovered from stress inversions of each cluster, in conjunction with the overall fault friction coefficient to estimate the effective differential stress required for frictional activation of areas that host SSEs. Zones of accumulated fault slip may be considered isotropic for the sake of simplicity or due to the assumption that successive slip has randomized the orientations of pores (or cracks) in the fault core (Healy, 2012). The governing assumption of isotropic poroelasticity is that fluids occupy equant pores and therefore the principal stresses are modulated by the pore fluid pressure, P_f, such that the effective principal stresses are $\sigma'_1 = \sigma_1 - P_f$, $\sigma'_2 = \sigma_2 - P_f$, and $\sigma'_3 = \sigma_3 - P_f$. In this case, frictional reactivation of a fault with static coefficient of friction, μ, is expressed as the frictional failure envelope, $\tau = \mu(\sigma_n - P_f)$, where τ and σ_n are the shear and normal stresses, respectively.

The frictional failure envelope may be expressed in terms of the principal effective stresses for the 2-D case as

$$(\sigma'_1 - \sigma'_3)\sin(2\theta) = \mu[(\sigma'_1 + \sigma'_3) - (\sigma'_1 - \sigma'_3)\cos(2\theta)] \tag{1}$$

where θ is the angle between σ_1 and the fault (Sibson, 1985). The effective differential stress required for reactivation of a thrust fault at depth, z, with near-vertical σ_3 is expressed as

$$(\sigma'_1 - \sigma'_3) = \frac{\mu(\cot\theta + \tan\theta)}{1 - \mu\tan\theta} \rho g z (1 - \lambda_v) \tag{2}$$

where ρ is the average rock density, g is the gravitational acceleration, and λ_v is the pore-fluid factor (Sibson, 1990). The pore-fluid factor is defined as the ratio of the pore fluid pressure to the vertical stress, $\lambda_v = P_f/\sigma_3$. We confirmed that σ_3 is near-vertical (Figures S4 and S5) and calculated the effective differential stress required for reactivation of each SSE cluster using the mean cluster depth, an average crustal density of 2.7 g/cm^3, a near-lithostatic pore-fluid factor of 0.99 (Bürgmann, 2018; Gao & Wang, 2017), and parameters recovered from the stress inversions: angles from σ_1 to the megathrust, the relative principal stress magnitudes, and the coefficient of friction. Additionally, we solve for the absolute effective maximum and minimum principal stresses by substituting Equation 2 into Equation 1.

The effective differential stress required for frictional reactivation for each SSE cluster ranges from 3.2 to 12.2 MPa, which is considerably weaker than observations and models of differential stress in the

lithosphere (Scholz, 2015; Zoback et al., 2002). Further, we find the maximum effective principal stress to be on the order of 10–20 MPa and the minimum effective principal stress to be on the order of 6–9 MPa, yielding values of effective mean stress ranging from 7.9 to 13.7 MPa. Overall, our findings suggest that the SSE source region is composed of intrinsically weak materials (e.g., $\mu = 0.19$–0.50) at high pore fluid pressures, resulting in slow fault slip due to absolute principal stresses on the order of several to tens of MPa.

5. Conclusions

We determine the deviatoric stress field of the Nankai Trough megathrust and interpret the results in the context of the regional tectonics. We find principal stress orientations in the central and eastern Nankai Trough that are consistent with a convergent margin and faulting on the megathrust and principal stress orientations in the western Nankai Trough that are consistent with subduction of the PS beneath an over-riding plate that hosts widespread extension in the forearc sliver. Short-term SSEs with a magnitude <6 are not completely represented by our compiled catalog, and shallow SSEs are poorly recovered by current geodetic studies. Given improved methods and instrument coverage that allow the detection of long-term, shallow, and low-magnitude SSEs, future stress analyses may reveal a more complete view of active tectonic stress fields. Our conclusions are summarized below.

1. Stress inversions typically employ catalogs of earthquake focal mechanisms to constrain regional stress orientations. In the Nankai Trough, SSEs release greater summed seismic moment than earthquakes for the same time period and have well-resolved focal mechanisms. As such, SSE focal mechanisms can be used to augment traditional focal mechanism catalogs resulting in better constrained estimates of stress field orientations and increased spatial resolution.
2. We find that creeping areas of the Nankai Trough subduction zone are well oriented for failure when both earthquakes and SSEs are considered in the inversions. Our results suggest that areas hosting SSEs and other slow fault slip may appear to have misoriented stress fields if slow fault slip is not included in the stress analysis.
3. The principal stress orientations of clusters of SSEs are well oriented for frictional failure with σ_1 at angles of 39.0° to 51.4° from the megathrust. From this we infer that the strength of the megathrust is similar to its surroundings. Low Vp/Vs ratios in the SSE source region and the modulation of slow slip by small applied stresses suggest the megathrust and surrounding faults operate at low deviatoric stresses.
4. Further, these angles imply friction coefficients between 0.19 and 0.50, suggesting that intrinsically low-strength materials are present in the SSE source region and surroundings in the Nankai Trough. Low fault friction coefficients and near-lithostatic pore fluid pressures in these regions imply low effective differential stress ($\sigma_1' - \sigma_3' = 3.2$–$12.2$ MPa) and effective mean stress (($\sigma_1' + \sigma_3'$)$/2 = 7.9$–13.7 MPa).

Data Availability Statement

All SSE data used in this study are openly available from the Slow Earthquake Database (https://www-solid.eps.s.u-tokyo.ac.jp/~sloweq). All earthquake focal mechanisms used in this study are openly available from the NIED Earthquake Mechanism Search (https://www.fnet.bosai.go.jp/event/search.php).

References

Álvarez-Gómez, J. A. (2019). FMC—Earthquake focal mechanisms data management, cluster and classification. *SoftwareX*, *9*, 299–307.

Anderson, E. M. (1951). *The dynamics of faulting and dyke formation with applications to Britain*. Edinburgh: Hafner Pub. Co. https://scits.stanford.edu/anderson-e-m-1951-dynamics-faulting-and-dyke-formation-applications-brittan-edinburgh-oliver-and

Angelier, J. (1984). Tectonic analysis of fault slip data sets. *Journal of Geophysical Research*, *89*, 5835–5848. https://doi.org/10.1029/JB089iB07p05835

Arnold, R., & Townend, J. (2007). A Bayesian approach to estimating tectonic stress from seismological data. *Geophysical Journal International*, *170*, 1336–1356. https://doi.org/10.1111/j.1365-246X.2007.03485.x

Arthur, D., & Vassilvitskii, S. (2006). K-means++: The advantages of careful seeding. In *Proceedings of the annual acm-siam symposium on discrete algorithms*. Stanford, CA: Stanford University. http://ilpubs.stanford.edu:8090/778/

Audet, P., & Bürgmann, R. (2014). Possible control of subduction zone slow-earthquake periodicity by silica enrichment. *Nature*, *510*, 389–392. https://doi.org/10.1038/nature13391

Bird, P. (2003). An updated digital model of plate boundaries. *Geochemistry, Geophysics, Geosystems*, *4*(3), 1027. https://doi.org/10.1029/2001GC000252

Bott, M. H. P. (1959). The mechanics of oblique slip faulting. *Geological Magazine*, *96*, 109–117. https://doi.org/10.1017/S0016756800059987

Brown, J. R., Beroza, G. C., Ide, S., Ohta, K., Shelly, D. R., Schwartz, S. Y., et al. (2009). Deep low-frequency earthquakes in tremor localize to the plate interface in multiple subduction zones. *Geophysical Research Letters*, *36*, L19306. https://doi.org/10.1029/2009GL040027

Brown, K. M., Kopf, A., Underwood, M. B., & Weinberger, J. L. (2003). Compositional and fluid pressure controls on the state of stress on the Nankai subduction thrust: A weak plate boundary. *Earth and Planetary Science Letters*, *214*, 589–603. https://doi.org/10.1016/S0012-821X(03)00388-1

Bürgmann, R. (2018). The geophysics, geology and mechanics of slow fault slip. *Earth and Planetary Science Letters*, *495*, 112–134. https://doi.org/10.1016/j.epsl.2018.04.062

Byerlee, J. (1978). Friction of rocks. In *Rock friction and earthquake prediction*. Basel: Birkhäuser. https://doi.org/10.1007/978-3-0348-7182-2_4

Byrne, T. B., Lin, W., Tsutsumi, A., Yamamoto, Y., Lewis, J. C., Kanagawa, K., et al. (2009). Anelastic strain recovery reveals extension across SW Japan subduction zone. *Geophysical Research Letters*, *36*, L23310. https://doi.org/10.1029/2009GL040749

Collettini, C., Tesei, T., Scuderi, M. M., Carpenter, B. M., & Viti, C. (2019). Beyond Byerlee friction, weak faults and implications for slip behavior. *Earth and Planetary Science Letters*, *519*, 1–316. https://doi.org/10.1016/j.epsl.2019.05.011

DeMets, C., Gordon, R. G., & Argus, D. F. (2010). Geologically current plate motions. *Geophysical Journal International*, *181*, 1–80. https://doi.org/10.1111/j.1365-246X.2009.04491.x

Dragert, H., Wang, K., & James, T. S. (2001). A silent slip event on the deeper Cascadia subduction interface. *Science*, *292*, 1525–1528. https://doi.org/10.1126/science.1060152

French, M. E., & Condit, C. B. (2019). Slip partitioning along an idealized subduction plate boundary at deep slow slip conditions. *Earth and Planetary Science Letters*, *528*, 1–10. https://doi.org/10.1016/j.epsl.2019.115828

Gao, X., & Wang, K. (2017). Rheological separation of the megathrust seismogenic zone and episodic tremor and slip. *Nature*, *543*, 416–419. https://doi.org/10.1038/nature21389

Gephart, J. W. (1990). Stress and the direction of slip on fault planes. *Tectonics*, *9*, 845–858. https://doi.org/10.1029/TC009i004p00845

Gephart, J. W., & Forsyth, D. W. (1984). An improved method for determining the regional stress tensor using earthquake focal mechanism data: Application to the San Fernando earthquake sequence. *Journal of Geophysical Research*, *89*, 9305–9320. https://doi.org/10.1029/JB089iB11p09305

Gutenberg, B., & Richter, C. F. (1944). Frequency of earthquakes in California. *Bulletin of the Seismological Society of America*, *34*(4), 185–188.

Hardebeck, J. L. (2015). Stress orientations in subduction zones and the strength of subduction megathrust faults. *Science*, *349*, 1213–1216. https://doi.org/10.1126/science.aac5625

Hardebeck, J. L., & Hauksson, E. (1999). Role of fluids in faulting inferred from stress field signatures. *Science*, *285*, 236–239. https://doi.org/10.1126/science.285.5425.236

Hardebeck, J. L., & Loveless, J. P. (2018). Creeping subduction zones are weaker than locked subduction zones. *Nature Geoscience*, *11*, 60–64. https://doi.org/10.1038/s41561-017-0032-1

Hardebeck, J. L., & Michael, A. J. (2004). Stress orientations at intermediate angles to the San Andreas Fault, California. https://doi.org/10.1029/2004JB003239

Hardebeck, J. L., & Michael, A. J. (2006). Damped regional-scale stress inversions: Methodology and examples for southern California and the Coalinga aftershock sequence. *Journal of Geophysical Research*, *111*, B11310. https://doi.org/10.1029/2005JB004144

Hawthorne, J. C., & Rubin, A. M. (2010). Tidal modulation of slow slip in Cascadia. *Journal of Geophysical Research*, *115*, B09406. https://doi.org/10.1029/2010JB007502

Hayes, G. P., Moore, G. L., Portner, D. E., Hearne, M., Flamme, H., Furtney, M., & Smoczyk, G. M. (2018). Slab2, a comprehensive subduction zone geometry model. *Science*, *362*, 58–61. https://doi.org/10.1126/science.aat4723

Healy, D. (2012). Anisotropic poroelasticity and the response of faulted rock to changes in pore-fluid pressure. *Geological Society Special Publication*, *367*, 201–214. https://doi.org/10.1144/SP367.14

Hill, D. P. (1993). A note on ambient pore pressure, fault-confined pore pressure, and apparent friction. *Bulletin of the Seismological Society of America*, *83*(2), 583–586.

Hirose, H., & Obara, K. (2005). Repeating short- and long-term slow slip events with deep tremor activity around the Bungo channel region, southwest Japan. *Earth, Planets and Space*, *57*, 961–972. https://doi.org/10.1186/BF03351875

Ikari, M. J., Saffer, D. M., & Marone, C. (2009). Frictional and hydrologic properties of a major splay fault system, Nankai subduction zone. *Geophysical Research Letters*, *36*, L20313. https://doi.org/10.1029/2009GL040009

Ikeda, M., Toda, S., Kobayashi, S., Ohno, Y., Nishizaka, N., & Ohno, I. (2009). Tectonic model and fault segmentation of the Median Tectonic Line active fault system on Shikoku, Japan. *Tectonics*, *28*, TC5006. https://doi.org/10.1029/2008TC002349

Itaba, S., Kitagawa, Y., Koizumi, N., Takahashi, M., Matsumoto, N., & Takeda, N. (2012). The variation of the strain, tilt and groundwater level in the Shikoku district and Kii peninsula, Japan (from may to october 2011). *Report of the Coordinating Committee for Earthquake Prediction*, *87*, 399–418.

Itaba, S., Kitagawa, Y., Koizumi, N., Takahashi, M., Matsumoto, N., & Takeda, N. (2013a). Short-term slow slip events in the Tokai area, the Kii peninsula and the Shikoku district, Japan (from May to October 2012). *Report of the Coordinating Committee for Earthquake Prediction*, *89*, 226–238.

Itaba, S., Kitagawa, Y., Koizumi, N., Takahashi, M., Matsumoto, N., & Takeda, N. (2013b). Short-term slow slip events in the Tokai area, the Kii peninsula and the Shikoku district, Japan (from November 2012 to April 2013). *Report of the Coordinating Committee for Earthquake Prediction*, *90*, 254–269.

Itaba, S., Koizumi, N., Takahashi, M., Matsumoto, N., Kitagawa, Y., Ochi, T., & Takeda, N. (2014). Short-term slow slip events in the Tokai area, the Kii peninsula and the Shikoku district, Japan (from November 2013 to April 2014). *Report of the Coordinating Committee for Earthquake Prediction*, *92*, 238–249.

Itaba, S., Koizumi, N., Takahashi, M., Matsumoto, N., Kitagawa, Y., & Takeda, N. (2014). Short-term slow slip events in the Tokai area, the Kii peninsula and the Shikoku district, Japan (from May to October 2013). *Report of the Coordinating Committee for Earthquake Prediction*, *91*, 230–242.

Ito, Y., Asano, Y., & Obara, K. (2009). Very-low-frequency earthquakes indicate a transpressional stress regime in the Nankai accretionary prism. *Geophysical Research Letters*, *36*, L20309. https://doi.org/10.1029/2009GL039332

Kagan, Y. Y. (2005). Double-couple earthquake focal mechanism: Random rotation and display. *Geophysical Journal International*, *164*, 236–245. https://doi.org/10.1111/j.1365-246X.2005

Kaneda, H., & Okada, A. (2008). Long-term seismic behavior of a fault involved in a multiple-fault rupture: Insights from tectonic geomorphology along the Neodani Fault, central Japan. *Bulletin of the Seismological Society of America*, *98*, 2170–2190. https://doi.org/10.1785/0120070204

Kano, M., Aso, N., Matsuzawa, T., Ide, S., Annoura, S., Arai, R., et al. (2018). Development of a slow earthquake database. *Seismological Research Letters*, *89*, 1566–1575. https://doi.org/10.1785/0220180021

Katsumata, A., & Kamaya, N. (2003). Low-frequency continuous tremor around the Moho discontinuity away from volcanoes in the southwest Japan. *Geophysical Research Letters*, *30*(1), 1020. https://doi.org/10.1029/2002GL015981

Kaverina, A. N., Lander, A. V., & Prozorov, A. G. (1996). Global creepex distribution and its relation to earthquake-source geometry and tectonic origin. *Geophysical Journal International*, *125*, 249–265. https://doi.org/10.1111/j.1365-246X.1996.tb06549.x

Kita, I., Yamamoto, M., Asakawa, Y., Nakagawa, M., Taguchi, S., & Hasegawa, H.(2001). Contemporaneous ascent of within-plate type and island-arc type magmas in the Beppu-Shimabara graben system, Kyushu island, Japan. *Journal of Volcanology and Geothermal Research*, *111*, 99. https://doi.org/10.1016/S0377-0273(01)00222-0

Kitagawa, Y., Itaba, S., Koizumi, N., Takahashi, M., Matsumoto, N., & Takeda, N. (2012). Short-term slow slip events in the Tokai area, the Kii peninsula and the Shikoku district, Japan (from November 2011 to April 2012). *Report of the Coordinating Committee for Earthquake Prediction*, *88*, 303–311.

Kitagawa, Y., Itaba, S., Takahashi, M., Matsumoto, N., & Takeda, N. (2011). The variation of the strain, tilt and groundwater level in the Shikoku district and Kii peninsula, japan (from November 2010 to May 2011). *Report of the Coordinating Committee for Earthquake Prediction*, *86*, 519–533.

Kobayashi, A. (2014). A long-term slow slip event from 1996 to 1997 in the Kii Channel, Japan. *Earth, Planets and Space*, *66*, 9. https://doi.org/10.1186/1880-5981-66-9

Kopf, A., & Brown, K. M. (2003). Friction experiments on saturated sediments and their implications for the stress state of the Nankai and Barbados subduction thrusts. *Marine Geology*, *202*, 193–210. https://doi.org/10.1016/S0025-3227(03)00286-X

Kubo, A., & Fukuyama, E. (2003). Stress field along the Ryukyu Arc and the Okinawa Trough inferred from moment tensors of shallow earthquakes. *Earth and Planetary Science Letters*, *310*, 305–316. https://doi.org/10.1016/S0012-821X(03)00132-8

Kubo, A., Fukuyama, E., Kawai, H., & Nonomura, K. (2002). NIED seismic moment tensor catalogue for regional earthquakes around Japan: Quality test and application. *Tectonophysics*, *356*, 23–48. https://doi.org/10.1016/S0040-1951(02)00375-X

Lee, J., Hong, T. K., & Chang, C. (2017). Crustal stress field perturbations in the continental margin around the Korean Peninsula and Japanese islands. *Tectonophysics*, *718*, 140–149. https://doi.org/10.1016/j.tecto.2017.08.003

Lin, W., Byrne, T. B., Kinoshita, M., McNeill, L. C., Chang, C., Lewis, J. C., et al. (2016). Distribution of stress state in the Nankai subduction zone, southwest Japan and a comparison with Japan Trench. *Tectonophysics*, *692*, 120–130. https://doi.org/10.1016/j.tecto.2015.05.008

Lombardi, A. M. (2017). SEDA: A software package for the Statistical Earthquake Data Analysis. *Scientific Reports*, *7*, 1–16. https://doi.org/10.1038/srep44171

Lund, B., & Slunga, R. (1999). Stress tensor inversion using detailed microearthquake information and stability constraints: Application to Ölfus in southwest Iceland. *Journal of Geophysical Research*, *104*, 14,947–14,964. https://doi.org/10.1029/1999JB900111

MATLAB (2018). *Version 9.4.0.813654 (r2018a)*. Natick, Massachusetts: The MathWorks Inc.

Martínez-Garzón, P., Ben-Zion, Y., Abolfathian, N., Kwiatek, G., & Bohnhoff, M. (2016). A refined methodology for stress inversions of earthquake focal mechanisms. *Journal of Geophysical Research: Solid Earth*, *121*, 8666–8687. https://doi.org/10.1002/2016JB013493

Martínez-Garzón, P., Kwiatek, G., Ickrath, M., & Bohnhoff, M. (2014). MSATSI: A MATLAB package for stress inversion combining solid classic methodology, a new simplified user-handling, and a visualization tool. *Seismological Research Letters*, *85*, 896–904. https://doi.org/10.1785/0220130189

Matsu'ura, M., & Hasegawa, Y. (1987). A maximum likelihood approach to nonlinear inversion under constraints. *Physics of the Earth and Planetary Interiors*, *47*, 179–187. https://doi.org/10.1016/0031-9201(87)90076-8

Maury, J., Cornet, F. H., & Dorbath, L. (2013). A review of methods for determining stress fields from earthquakes focal mechanisms; Application to the Sierentz 1980 seismic crisis (Upper Rhine Graben). https://doi.org/10.2113/gssgfbull.184.4-5.319

McKenzie, D. P. (1969). Relation between fault plane solutions for earthquakes and the directions of the principal stresses. *Bulletin of the Seismological Society of America*, *29*, 189–193. https://doi.org/10.1136/bmj.2.3908.1076

Michael, A. J. (1984). Determination of stress from slip data: Faults and folds. *Journal of Geophysical Research*, *89*, 11,517–11,526. https://doi.org/10.1029/JB089iB13p11517

Miyazaki, S., & Heki, K. (2001). Crustal velocity field of southwest Japan: Subduction and arc-arc collision. *Journal of Geophysical Research*, *106*, 4305–4326. https://doi.org/10.1029/2000JB900312

Nadeau, R. M., & Dolenc, D. (2005). Nonvolcanic tremors deep beneath the San Andreas Fault. *Science*, *307*, 389. https://doi.org/10.1126/science.1107142

Nishimura, T. (2014). Short-term slow slip events along the Ryukyu Trench, southwestern Japan, observed by continuous GNSS. *Progress in Earth and Planetary Science*, *1*, 22. https://doi.org/10.1186/s40645-014-0022-5

Nishimura, T., Matsuzawa, T., & Obara, K. (2013). Detection of short-term slow slip events along the Nankai Trough, southwest Japan, using GNSS data. *Journal of Geophysical Research: Solid Earth*, *118*, 3112–3125. https://doi.org/10.1002/jgrb.50222

Obara, K. (2002). Nonvolcanic deep tremor associated with subduction in southwest Japan. *Science*, *296*, 1679–1681. https://doi.org/10.1126/science.1070378

Obara, K., Hirose, H., Yamamizu, F., & Kasahara, K. (2004). Episodic slow slip events accompanied by non-volcanic tremors in southwest Japan subduction zone. *Geophysical Research Letters*, *31*, L23602. https://doi.org/10.1029/2004GL020848

Obara, K., & Ito, Y. (2005). Very low frequency earthquakes excited by the 2004 off Kii peninsula earthquakes: A dynamic deformation process in the large accretionary prism. *Earth, Planets and Space*, *57*, 321–326. https://doi.org/10.1186/BF03352570

Ochi, T., Itaba, S., Koizumi, N., Takahashi, M., Matsumoto, N., Kitagawa, Y., & Takeda, N. (2015). Short-term slow slip events in the Tokai area, the Kii peninsula and the Shikoku district, Japan (from November 2014 to April 2015). *Report of the Coordinating Committee for Earthquake Prediction*, *94*, 250–261.

Ochi, T., Itaba, S., Koizumi, N., Takahashi, M., Matsumoto, N., Kitagawa, Y., & Takeda, N. (2016). Short-term slow slip events in the Tokai area, the Kii peninsula and the Shikoku district, Japan (from May 2015 to October 2015). *Report of the Coordinating Committee for Earthquake Prediction*, *95*, 255–264.

Okada, Y., Kasahara, K., Hori, S., Obara, K., Sekiguchi, S., Fujiwara, H., & Yamamoto, A. (2004). Recent progress of seismic observation networks in Japan—Hi-net, F-net, K-net and KiK-net. *Earth, Planets and Space*, *56*, xv–xxviii. https://doi.org/10.1186/BF03353076

Pawlowicz, R. (2019). M_map: A mapping package for Matlab, version 1.4k. www.eoas.ubc.ca/~rich/map.html

Payero, J. S., Kostoglodov, V., Shapiro, N., Mikumo, T., Iglesias, A., Pérez-Campos, X., & Clayton, R. W. (2008). Nonvolcanic tremor observed in the Mexican subduction zone. *Geophysical Research Letters*, *35*, L07305. https://doi.org/10.1029/2007GL032877

Reid, H. F. (1910). The California earthquake of April 18, 1906. *Report of the State Earthquake Investigation Commission*, *2*, 16–18.

Research Information Database DB095: Active fault database of Japan (2012). National Institute of Advanced Industrial Science and Technology https://gbank.gsj.jp/activefault/index_e_gmap.html

Rogers, G., & Dragert, H. (2003). Episodic tremor and slip on the Cascadia subduction zone: The chatter of silent slip. *Science*, *300*, 1942–1943. https://doi.org/10.1126/science.1084783

Sacks, A., Saffer, D. M., & Fisher, D. (2013). Analysis of normal fault populations in the Kumano forearc basin, Nankai Trough, Japan: 2. Principal axes of stress and strain from inversion of fault orientations. *Geochemistry, Geophysics, Geosystems*, *14*, 1973–1988. https://doi.org/10.1002/ggge.20118

Sagiya, T., Miyazaki, S., & Tada, T. (2000). Continuous GPS array and present-day crustal deformation of Japan. *Pure and Applied Geophysics*, *157*, 2303–2322. https://doi.org/10.1007/978-3-0348-7695-7_26

Scholz, C. H. (2015). On the stress dependence of the earthquake b value. *Geophysical Research Letters*, *42*, 1399–1402. https://doi.org/10.1002/2014GL062863

Sekine, S., Hirose, H., & Obara, K. (2010). Along-strike variations in short-term slow slip events in the southwest Japan subduction zone. *Journal of Geophysical Research*, *115*, B00A27. https://doi.org/10.1029/2008JB006059

Shelly, D. R., Beroza, G. C., & Ide, S. (2007). Non-volcanic tremor and low-frequency earthquake swarms. *Nature*, *446*, 305–307. https://doi.org/10.1038/nature05666

Shen, L. W., Schmitt, D. R., & Haug, K. (2019). Quantitative constraints to the complete state of stress from the combined borehole and focal mechanism inversions: Fox Creek, Alberta. *Tectonophysics*, *764*, 110–123. https://doi.org/10.1016/j.tecto.2019.04.023

Sibson, R. H. (1985). A note on fault reactivation. *Journal of Structural Geology*, *7*(6), 751–754. https://doi.org/10.1016/0148-9062(92)91063-b

Sibson, R. H. (1990). Rupture nucleation on unfavourably oriented faults. *Bulletin—Seismological Society of America*, *7*, 751–754. https://doi.org/10.1016/0191-8141(85)90150-6

Tada, T. (1985). Spreading of the Okinawa Trough and its relation to the crustal deformation in the Kyushu (2). *Zisin (Journal of the Seismological Society of Japan. 2nd ser.)*, *51*, 113–121. https://doi.org/10.4294/zisin1948.38.1_1

Takemura, S., Matsuzawa, T., Noda, A., Tonegawa, T., Asano, Y., Kimura, T., & Shiomi, K. (2019). Structural characteristics of the Nankai Trough shallow plate boundary inferred from shallow very low frequency earthquakes. *Geophysical Research Letters*, *46*, 4192–4201. https://doi.org/10.1029/2019GL082448

Terakawa, T., & Matsu'ura, M. (2010). The 3-D tectonic stress fields in and around Japan inverted from centroid moment tensor data of seismic events. *Tectonics*, *29*, TC6008. https://doi.org/10.1029/2009TC002626

Thomas, A. M., Bürgmann, R., Shelly, D. R., Beeler, N. M., & Rudolph, M. L. (2012). Tidal triggering of low frequency earthquakes near Parkfield, California: Implications for fault mechanics within the brittle-ductile transition. *Journal of Geophysical Research*, *117*, B05301. https://doi.org/10.1029/2011jb009036

Tobin, H. J., & Saffer, D. M. (2009). Elevated fluid pressure and extreme mechanical weakness of a plate boundary thrust, Nankai Trough subduction zone. *Geology*, *37*, 679–682. https://doi.org/10.1130/G25752A.1

Townend, J., & Zoback, M. D. (2001). Implications of earthquake focal mechanisms for the frictional strength of the San Andreas fault system. *Geological Society Special Publication*, *186*, 13. https://doi.org/10.1144/GSL.SP.2001.186.01.02

Townend, J., & Zoback, M. D. (2006). Stress, strain, and mountain building in central Japan. *Journal of Geophysical Research*, *111*, B03411. https://doi.org/10.1029/2005JB003759

Tsutsumi, H., Okada, A., Nakata, T., Ando, M., & Tsukuda, T. (1991). Timing and displacement of holocene faulting on the median tectonic line in central Shikoku, southwest Japan. *Journal of Structural Geology*, *13*, 227–233. https://doi.org/10.1016/0191-8141(91)90069-U

Ujiie, K., Saishu, H., Fagereng, Å., Nishiyama, N., Otsubo, M., Masuyama, H., & Kagi, H. (2018). An explanation of episodic tremor and slow slip constrained by crack-seal veins and viscous shear in subduction mélange. *Geophysical Research Letters*, *45*, 5371–5379. https://doi.org/10.1029/2018GL078374

Usami, T. (1996). *Materials for comprehensive list of destructive earthquakes in Japan, 416-1995* (Revised and Enlarged Edition). Tokyo, Japan: University of Tokyo Press.

Vavryčuk, V. (2014). Iterative joint inversion for stress and fault orientations from focal mechanisms. *Geophysical Journal International*, *199*, 69–77. https://doi.org/10.1093/gji/ggu224

Vavryčuk, V., Bouchaala, F., & Fischer, T. (2013). High-resolution fault image from accurate locations and focal mechanisms of the 2008 swarm earthquakes in West Bohemia, Czech Republic. *Tectonophysics*, *590*, 189–195. https://doi.org/10.1016/j.tecto.2013.01.025

Wallace, R. E. (1951). Geometry of shearing stress and relation to faulting. *The Journal of Geology*, *59*, 118–130. https://doi.org/10.1086/625831

Wang, K., Wada, I., & Ishikawa, Y. (2004). Stresses in the subducting slab beneath southwest Japan and relation with plate geometry, tectonic forces, slab dehydration, and damaging earthquakes. *Journal of Geophysical Research*, *109*, B08304. https://doi.org/10.1029/2003JB002888

Warren-Smith, E., Fry, B., Wallace, L., Chon, E., Henrys, S., Sheehan, A., et al. (2019). Episodic stress and fluid pressure cycling in subducting oceanic crust during slow slip. *Nature Geoscience*, *12*, 475–481. https://doi.org/10.1038/s41561-019-0367-x

Wech, A. G., Creager, K. C., Houston, H., & Vidale, J. E. (2010). An earthquake-like magnitude-frequency distribution of slow slip in northern Cascadia. *Geophysical Research Letters*, *37*, L22310. https://doi.org/10.1029/2010GL044881

Wessel, P., Smith, W. H. F., Scharroo, R., Luis, J., & Wobbe, F. (2013). Generic mapping tools: Improved version released. *Eos*, *94*, 409–410. https://doi.org/10.1002/2013EO450001

Yokota, Y., Ishikawa, T., Watanabe, S. I., Tashiro, T., & Asada, A. (2016). Seafloor geodetic constraints on interplate coupling of the Nankai Trough megathrust zone. *Nature*, *534*, 374–377. https://doi.org/10.1038/nature17632

Zhuang, J., Ogata, Y., & Vere-Jones, D. (2002). Stochastic declustering of space-time earthquake occurrences. *Journal of the American Statistical Association*, *97*, 369–380. https://doi.org/10.1198/016214502760046925

Zoback, M. D., Townend, J., & Grollimund, B. (2002). Steady-state failure equilibrium and deformation of intraplate lithosphere. *International Geology Review*, *44*, 383–401. https://doi.org/10.2747/0020-6814.44.5.383

Zonenshain, L. P., & Savostin, L. A. (1981). Geodynamics of the Baikal rift zone and plate tectonics of Asia. *Tectonophysics*, *76*, 1–45. https://doi.org/10.1016/0040-1951(81)90251